Structurally optimized sandwich panels with prismatic cores

L. Valdevit [a,*], J.W. Hutchinson [b], A.G. Evans [c]

[a] *Department of Mechanical and Aerospace Engineering, Princeton University, Princeton, NJ 08540, USA*
[b] *Division of Engineering and Applied Sciences, Harvard University, Cambridge, MA 02139, USA*
[c] *Materials Department, University of California at S. Barbara, S. Barbara, CA 93106, USA*

Abstract

Multifunctional sandwich panels with corrugated and prismatic diamond cores have been analyzed and their behavior compared with panels designed using truss and honeycomb cores. Failure mechanism maps have been devised that account for interactions between core and face members during buckling. The optimal dimensions and the minimum weight have been evaluated. The load capacities predicted for near-optimal designs have been validated by conducting selected finite element calculations. Designs that use diamond prismatic cores (with corrugation order 4) are slightly more weight efficient than trusses, when optimized for a specific loading direction. Honeycomb cores, while somewhat more weight efficient, especially at lower load capacities, are not amenable to the fluid flows needed for cooling. We conclude that the diamond prismatic topology is the most weight efficient among designs amenable to simultaneous load bearing and active cooling.
© 2004 Elsevier Ltd. All rights reserved.

Keywords: Ultra-lightweight structures; Prismatic sandwich panels; FEM; Buckling; Optimal design

1. Introduction

The attributes of all-metallic sandwich panels with truss and prismatic cores have been outlined in prior assessments (Allen, 1969; Ashby et al., 2000; Chiras et al., 2002; Gibson and Ashby, 1999; Lu, 2001; Wicks and Hutchinson, 2001; Wicks and Hutchinson, 2004; Zok et al., 2003). When configured as flat plates loaded in bending, designs based on honeycomb cores have not been surpassed for structural efficiency. The situation changes when the panels are curved. Then, alternative cores become competitive, because the performance of honeycomb core panels is sensitive to misalignment. Alternatives may also be preferred when multifunctionality, such as cooling and energy absorption, as well as manufacturing cost, are addressed. To realize active cooling, it must be possible to flow a fluid through the core: requiring open, continuous channels.

---

[*] Corresponding author. Tel.: +1-617-496-7107; fax: +1-617-496-0601.
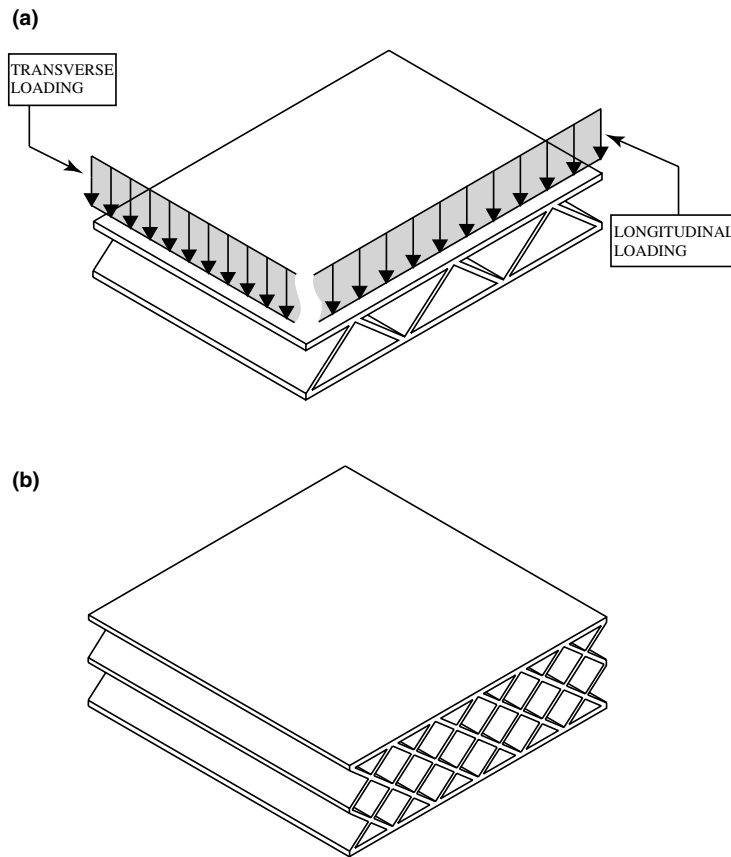*E-mail address:* valdevit@princeton.edu (L. Valdevit).

Fig. 1. Schematic of a prismatic panel: (a) corrugated core ($n = 1$) and (b) diamond core ($n = 4$). The two loading directions are depicted.

This article extends the understanding of topological possibilities for open cores by analyzing the structural efficiency of corrugated and diamond prismatic designs (Fig. 1) within a framework similar to that demonstrated for truss cores (Wicks and Hutchinson, 2001). Emphasis is placed on panels subject to out of plane bending. Two loading directions (referred to as transverse and longitudinal) were studied (Fig. 1a). The primary goal is to find designs that minimize the weight needed to support the bending loads without failure. The results cover a wide enough range of core relative densities, $\bar{\rho}$, to influence subsequent thermo-mechanical optimization, recognizing that the cooling efficiency optimum occurs at $\bar{\rho} \approx 0.1$ (Fig. 2) (Gu et al., 2001).

The present assessment is conducted as follows. In each loading direction all failure mechanisms are identified (face yielding, face buckling, core yielding and core buckling), and analytical expressions derived for the critical loads. Selected finite element results are used to check the applicability of the analytic solutions. Non-dimensional expressions are obtained for the combination of bending moment and shear force that activates each failure mechanism. A quadratic optimizer is used to ascertain the dimensions that minimize the panel weight at representative loads, subject to the constraint that the ratio of the panel thickness to span should not exceed an allowable maximum (Wicks and Hutchinson, 2001). The consequent structural efficiencies are compared with those for other core topologies, especially truss and honeycomb cores.
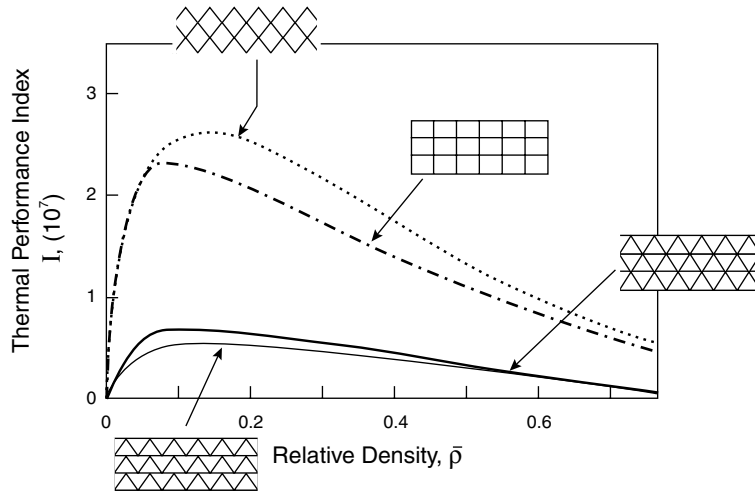
Fig. 2. The thermal performance of various prismatic cores. The ordinate is a thermal index, I, which is a measure of the ratio of the heat transfer rate to the pumping power (Gu et al., 2001). Note that the thermal index for the diamond core has a maximum for a relative density of about 8%.

The outline of the paper is as follows. In Section 2 we derive the critical loads for a panel loaded transversely, and in Section 3 we use a similar (although somewhat more involved) analysis to obtain the equivalent loads for the longitudinal direction. Section 4 presents the results of the weight minimization; maps that graphically depict the failure mechanisms are presented in Section 5. Finally, Section 6 offers a comparison of analytical results and finite element simulations. Implications and conclusions follow.

2. Failure mechanisms in transverse loading

The geometry to be addressed (Fig. 3) uses d as the face sheet thickness, d_c the core member thickness and H the overall panel height, with n the order of corrugation. The angle θ between the folded core plate and the horizontal is set to $\theta = \tan^{-1}\sqrt{2} \cong 54.7°$, since this angle maximizes the transverse shear stiffness (Lu, 2001). The panel supports a maximum moment, M, and shear force, V, both per unit width. The panel and the individual members are slender: whereupon the shear force is carried almost entirely by the core and the moment almost entirely by the face sheets (Wicks and Hutchinson, 2001). This treatment allows any combination of moment and shear force to be expressed by the length parameter $\ell = M/V$. All results refer to panels with both face sheets having the same thickness, as well as core and faces made from the same material.

The maximum stresses in the members are (Lu, 2001): for the face sheet,

$$\sigma_f = \frac{M}{d(H-d)} = \frac{V\ell}{d(H-d)} \tag{1a}$$

and for the core,

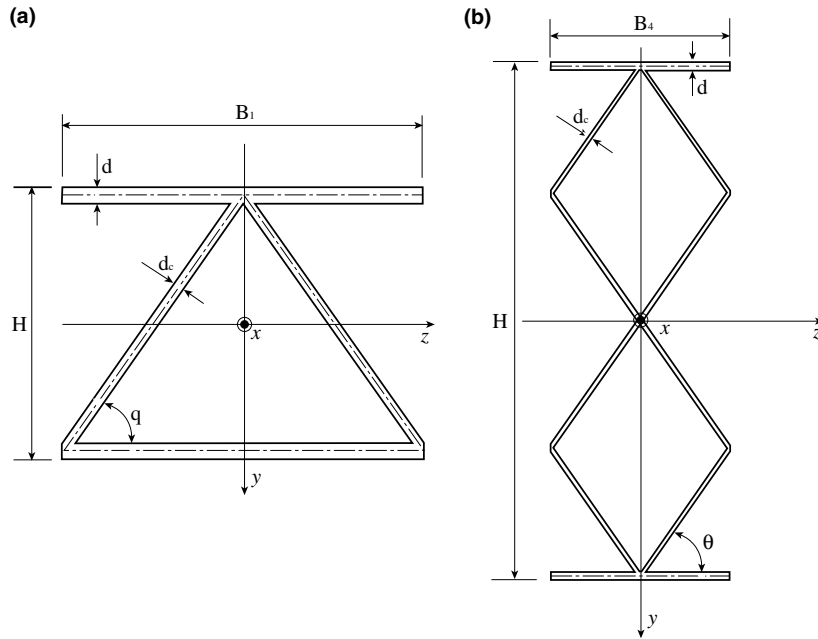$$\sigma_c = \frac{1}{n \sin\theta} \frac{V}{d_c}. \tag{1b}$$

Fig. 3. Schematic of a unit cell for (a) corrugated and (b) diamond ($n = 4$) core panels. The coordinate system and the geometric parameters are depicted.

The critical stresses are (Lu, 2001):

$$\sigma_f = \sigma_Y \quad \text{face sheet yielding,}$$

$$\sigma_f = \frac{k_f \pi^2 E I_f}{\lambda_f^2 d} \quad \text{face sheet buckling,}$$

$$\sigma_c = \sigma_Y \quad \text{core member yielding,}$$

$$\sigma_c = \frac{k_c \pi^2 E I_c}{\lambda_c^2 d_c} \quad \text{core member buckling,}$$

(2)

where λ_f and λ_c are the lengths of the face sheet and core plate members ($\lambda_f = 2(H - d)/n \tan \theta$, $\lambda_c = (H - d)/n \sin \theta$), σ_Y is the yield strength, and E the Young's modulus, while I_f and I_c are the moments of area per unit width for the face member and the core member, respectively ($I_f = d^3/12$, $I_c = d_c^3/12$). It will emerge from the optimizations that face and core buckling are always simultaneously active at the minimum weight configuration: placing an onus on the treatment used to characterize buckling.

To obtain the buckling coefficients, k_f and k_c, both the face and core members are treated as slender columns supported at their ends by two torsional springs. The stiffness of these springs is adjusted to simulate the constraint offered by the adjoining members (Bazant and Cedolin, 1991; Lu, 2001; Tall, 1974; Wiernicki et al., 1991). Preliminary assessments using finite elements (see Section 6) have revealed that, to obtain satisfactory solutions, the stiffness offered by adjoining members on the verge of buckling must be excluded. Otherwise the loads are non-conservative.

2.1. Face members

To calculate the torsional stiffness for face members in compression, we adopt the following strategy. We retain only the end support provided by one core member since, around the optimum, the other is close to buckling. For the same reason, the constraints offered by the adjoining face members are neglected. The torsional stiffness is then (Fig. 4a):
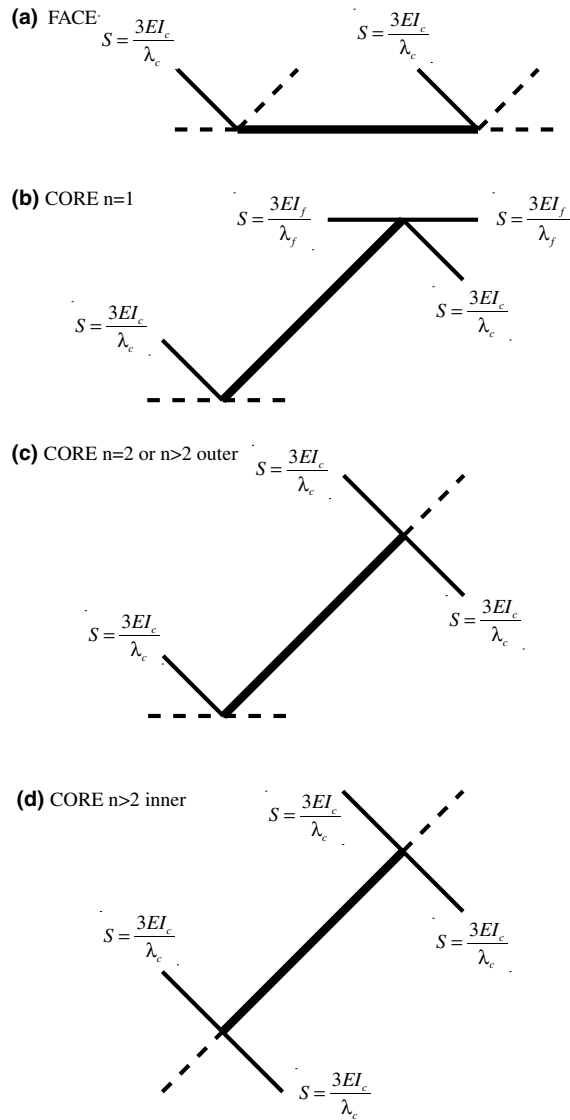

Fig. 4. Schematic of the procedure employed to calculate the torsional stiffness at the end of each member. The thick line represents the member under consideration; the thin dashed lines represent adjoining members that might be on the verge of buckling and whose contribution to the torsional stiffness is neglected; the thin solid line represents adjoining members that are in tensions: their contribution is indicated.

$$S_{f,1} = S_{f,2} = \frac{3EI_c}{\lambda_c}. \tag{3}$$

The factor 3 emerges if the constraining members are considered to be pin jointed.

2.2. Core members

For a corrugated core panel ($n = 1$), the compressed core members have different constraints at the two ends. At one end, support is provided by the adjacent core member plus two face members. At the other end, the adjoining face members are close to buckling, whereupon the only effective constraint is that offered by the adjacent core member. Hence (Fig. 4b):

$$S_{c,1}^{corr} = 2\frac{3EI_f}{\lambda_f} + \frac{3EI_c}{\lambda_c}, \tag{4a}$$

$$S_{c,2}^{corr} = \frac{3EI_c}{\lambda_c}. \tag{4b}$$

For a diamond core plate with $n = 2$, members most prone to buckling (those near the compression face) are constrained by the core member in contact with the faces as well as two core members at the neutral plane. Hence (Fig. 4c):

$$S_{c,1}^{n=2} = \frac{3EI_c}{\lambda_c}, \tag{5a}$$

$$S_{c,2}^{n=2} = 2\frac{3EI_c}{\lambda_c}. \tag{5b}$$

For a diamond core plate with $n > 2$, the buckling of the inner core members is subject a stiffness at both ends, $S_{c,2}^{n=2}$ (Fig. 4d). Note that the outer member is always less constrained that the inner, thus allowing Eq. (5) to be used for any corrugation.

For all the cases of interest, the buckling coefficients are estimated by inserting the preceding stiffness values into the approximate formulae (Bazant and Cedolin, 1991):

$$k_f = \frac{(0.4 + \eta_{f,1})(0.4 + \eta_{f,2})}{(0.2 + \eta_{f,1})(0.2 + \eta_{f,2})}, \quad k_c = \frac{(0.4 + \eta_{c,1})(0.4 + \eta_{c,2})}{(0.2 + \eta_{c,1})(0.2 + \eta_{c,2})}, \tag{6}$$

where

$$\eta_{f,i} = \frac{EI_f}{\lambda_f S_{f,i}}, \quad \eta_{c,i} = \frac{EI_c}{\lambda_c S_{c,i}} \tag{7}$$

such that

$$k_f = \left(\frac{2.4\cos\theta(d_c/d)^3 + 1}{1.2\cos\theta(d_c/d)^3 + 1}\right)^2, \tag{8a}$$

$$k_c^{corr} = 1.375\left(\frac{2.2 + 1.2(d/d_c)^3/\cos\theta}{1.6 + 0.6(d/d_c)^3/\cos\theta}\right), \tag{8b}$$

$$k_c^{diam} = 2.125. \tag{8c}$$

These buckling coefficients will be used in all the subsequent calculations.

The four failure criteria, re-written in the non-dimensional form used to construct mechanism maps, become

$$\frac{V^2}{EM} = \frac{\sigma_Y}{E} \frac{d}{\ell} \left(\frac{H}{\ell} - \frac{d}{\ell} \right) \quad \text{face yielding,}$$

$$\frac{V^2}{EM} = n \sin \theta \frac{\sigma_Y}{E} \frac{d_c}{\ell} \quad \text{core yielding,}$$

$$\frac{V^2}{EM} = \frac{k_f \pi^2}{48} n^2 \tan^2 \theta \left(\frac{H}{\ell} - \frac{d}{\ell} \right)^{-1} \left(\frac{d}{\ell} \right)^3 \quad \text{face buckling,}$$

$$\frac{V^2}{EM} = \frac{k_c \pi^2}{12} n^3 \sin^3 \theta \left(\frac{H}{\ell} - \frac{d}{\ell} \right)^{-2} \left(\frac{d_c}{\ell} \right)^3 \quad \text{core buckling.}$$

(9)

The influence of the material properties and loads are fully-embodied within the two non-dimensional quantities: σ_Y/E, and, V^2/EM. The non-dimensional geometric parameters are d/ℓ, d_c/ℓ, H/ℓ, n.

3. Failure mechanisms in longitudinal loading

3.1. Stresses in the faces and the core

For the longitudinal orientation, it is not legitimate to assume that the shear force is carried entirely by the core and the moment by the faces. Instead, the full stress distribution at any plane in the most heavily loaded cross section needs to be evaluated. Accordingly, the results only apply when the maximum moment and shear force occur at the same cross section. This would be the case for thin panels subject to either a cantilever load or three-point bending. Subject to this restriction, some general results are derived first for the normal stresses associated with M and the shear stress dictated by V, using the coordinates depicted on Fig. 3. The width of the unit cell considered depends on the order of corrugation n, and is given by

$$B_n = \frac{2(H - d)}{n \tan \theta}. \tag{10}$$

The maximum moment induces the normal stress:

$$\sigma = \frac{MB_n}{I_L} y, \tag{11}$$

where I_L represents the moment of area of the section. Retaining only leading order terms, and neglecting any contribution of relative order d/H and d_c/H, gives

$$I_L = \frac{1}{2} B_n d(H - d)^2 + \frac{1}{6 \sin \theta} d_c (H - d)^3. \tag{12}$$

For thin-walled sections, the stress induced by the shear force is tangential to the wall and given by (Den Hartog, 1949):

$$\tau = \frac{VB_n}{I_L b} \int_{y_0}^{(H-d)/2} y \, dA, \tag{13}$$

with y_0 the location where the stress is computed, and b the thickness of the wall at that point. In the faces, the shear stress is linear in z in the unit cell:

$$\tau_f = \frac{V\left(\frac{1}{n\tan\theta} - z/(H-d)\right)}{d + \frac{n}{6\cos\theta}d_c} \tag{14a}$$

and parabolic in y in the core:

$$\tau_c = \frac{V\left[\frac{1}{2n\tan\theta}\frac{d}{d_c} + \frac{1}{2\sin\theta}\left(\frac{1}{4} - \left(\frac{y}{H-d}\right)^2\right)\right]}{\frac{1}{2}d + \frac{n}{12\cos\theta}d_c}. \tag{14b}$$

A sketch of the shear stress distribution is provided in Fig. 5.

In the *faces* the normal stress σ_f is uniform along z and a shear stress τ_f is maximum at the center of the faces ($z = 0$). The stress at this location is

$$\sigma_f = \frac{V\ell}{d(H-d) + \frac{n}{6\cos\theta}d_c(H-d)},$$
$$\tau_f = \frac{V}{n\tan\theta d + \frac{n^2\tan\theta}{6\cos\theta}d_c} = \sigma_f\frac{1}{n\tan\theta}\frac{H-d}{\ell}. \tag{15}$$

In the core, the normal stress is maximum at the points of contact with the face sheets ($y = H/2 - d$), the shear stress is maximum at the center ($y = 0$). The stress at any point is

$$\sigma_c = \frac{2V\ell/(H-d)^2}{d + \frac{n}{6\cos\theta}d_c}y,$$
$$\tau_c = \frac{V\left[\frac{1}{n\tan\theta}\frac{d}{d_c} + \frac{1}{\sin\theta}\left(\frac{1}{4} - \left(\frac{y}{H-d}\right)^2\right)\right]}{d + \frac{n}{6\cos\theta}d_c}, \tag{16}$$

where y varies from 0 to $H/2 - d$.

3.2. Failure by yielding

The Mises criterion for face and core yield is $\sigma^2 + 3\tau^2 = \sigma_Y^2$. For the *faces*, substituting the stress components from (15) gives
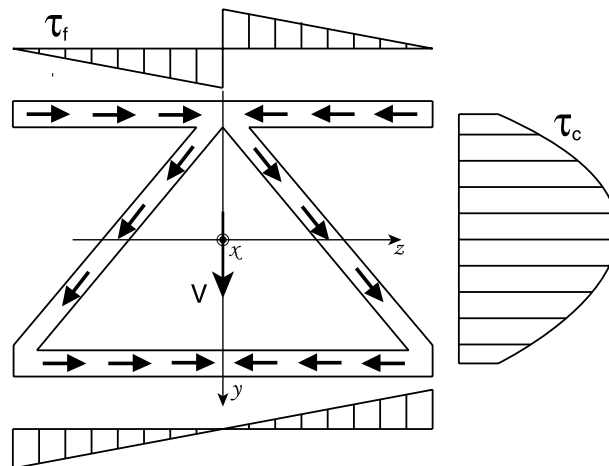

Fig. 5. Shear stress diagram for a thin-walled corrugated core plate. The same distribution applies to diamond core panels ($n \neq 1$).

$$\left(\frac{V^2}{EM}\right)_{\text{face yielding}} = \frac{\frac{\sigma_Y}{E}\left(\frac{H}{\ell}-\frac{d}{\ell}\right)\left[n\frac{d}{\ell}+\frac{n^2}{6\cos\theta}\frac{d_c}{\ell}\right]}{\sqrt{n^2+\frac{3}{\tan^2\theta}\left(\frac{H}{\ell}-\frac{d}{\ell}\right)^2}}. \tag{17}$$

For the *core*, since the location of the maximum Mises stress is unknown a priori, the yield condition is

$$\left(\frac{V^2}{EM}\right)_{\text{core yielding}} = \min_{y\in\left[0,\frac{H}{2}-d\right]}\left\{\frac{\frac{\sigma_Y}{E}\left(\frac{H}{\ell}-\frac{d}{\ell}\right)\left[\frac{d}{\ell}+\frac{n}{6\cos\theta}\frac{d_c}{\ell}\right]}{\sqrt{4\left(\frac{y}{H-d}\right)^2+3\left[\frac{1}{n\tan\theta}\left(\frac{H}{\ell}-\frac{d}{\ell}\right)\frac{d}{\ell}\frac{\ell}{d_c}+\frac{1}{\sin\theta}\left(\frac{H}{\ell}-\frac{d}{\ell}\right)\left(\frac{1}{4}-\left(\frac{y}{H-d}\right)^2\right)\right]^2}}\right\}. \tag{18}$$

3.3. Failure by buckling

To estimate the buckling loads, the face sheet is regarded as an isolated plate, width $\lambda_f = 2(H-d)/n\tan\theta$, and length much greater than the width. The two short edges are taken to be uniformly loaded in compression (neglecting the stress variation across the thickness). The limiting constraints on the long edges are simply supported and fully clamped. The former underestimates the critical load, thus yielding a conservative prediction; whereas the latter overestimates it. Finite element calculations (see Section 6) have revealed that the simply supported assumption provides the most realistic estimates. The normal stress at buckling is (the influence of shear stress is neglected) (Allen and Bulson, 1980):

$$\sigma_f^{cr} = \frac{K_c\pi^2 E}{12(1-v^2)}\left(\frac{d}{\lambda_f}\right)^2, \tag{19}$$

where

$K_c = 4$ for simply supported edges,

$K_c = 6.97$ for fully clamped edges.

Equating to the normal stress yields a *face* buckling condition:

$$\left(\frac{V^2}{EM}\right)_{\text{face buckling}} = \frac{K_c\pi^2}{24(1-v^2)}n^2\tan^2\theta\left(\frac{d}{\ell}\right)^2\left(\frac{H}{\ell}-\frac{d}{\ell}\right)^{-1}\left[\frac{1}{2}\frac{d}{\ell}+\frac{n}{12\cos\theta}\frac{d_c}{\ell}\right]. \tag{20}$$

For the core members, the shear and normal components of the stress are of the same order, and both need to be considered. We idealize the core members as isolated plates, width $\lambda_c = (H-d)/n\sin\theta$, and length much greater than the width, subject to a combination of shear and normal stress along the short sides.

For a corrugated panel ($n = 1$), the shear stress is taken to be uniform and equal to its maximum; the linear variation of the normal stress along the short side (from $-\sigma_c^{max}$ to $+\sigma_c^{max}$) is retained, but that along the long side is neglected.

The critical shear stress (no normal stress acting) is

$$\tau_c^{cr} = \frac{K_s\pi^2 E}{12(1-v^2)}\left(\frac{d_c}{\lambda_c}\right)^2, \tag{21}$$

where (Allen and Bulson, 1980; Southwell and Skan, 1924)

$K_s = 5.35$ for simply supported edges,

$K_s = 8.98$ for fully clamped edges.

The critical normal stress alone (no shear stress acting) is

$$\sigma_c^{cr} = \frac{K_b \pi^2 E}{12(1-v^2)} \left(\frac{d_c}{\lambda_c}\right)^2,$$

(22)

where

$K_b = 23.9$ for simply supported edges (Allen and Bulson, 1980),

$K_b = 41.5$ for fully clamped edges (Leissa and Kang, 2002).

For a diamond core panel with $n = 2$, we again assume that the shear stress in the core member is uniform and equal to its maximum value, but we realize that the normal stress now varies between $-\sigma_c^{max}$ and 0 along the short side (and as we did before, we neglect any stress variation along the long side). The equation governing the critical shear stress is the same as before, whereas the critical normal stress is given by

$$\sigma_c^{cr} = \frac{K_{bc} \pi^2 E}{12(1-v^2)} \left(\frac{d_c}{\lambda_c}\right)^2,$$

(23)

where

$K_{bc} = 7.81$ for simply supported edges (Allen and Bulson, 1980),

$K_{bc} = 13.6$ for fully clamped edges (Leissa and Kang, 2002).

For a diamond core panel with $n > 2$, two scenarios must be considered: (i) buckling of an inner core member (i.e. a member with one end lying on the neutral axis), and (ii) buckling of an outer core member (i.e. a member connected with the face sheet). Note that case (i) is governed mainly by shear buckling, whereas case (ii) is governed mainly by compression buckling. For case (i), the shear stress is treated as uniform and equal to its maximum value (the value at the neutral axis), whereas the linear variation of the normal stress along the short side is retained (the stress varying from $\sigma_c = 0$ to $\sigma_c = 2\sigma_c^{max}/n$). The critical stresses are the same as for the case $n = 2$ (Eq. (23)), although the applied normal stress is scaled by the quantity $2/n$.

For case (ii), we treat the normal stress as uniform along both sides and equal to its maximum value, and the shear stress as uniform along both sides and equal to its minimum value (the value at the node). The equation governing the shear stress is again the same, and the one governing the normal stress is

$$\sigma_c^{cr} = \frac{K_c \pi^2 E}{12(1-v^2)} \left(\frac{d_c}{\lambda_c}\right)^2,$$

(24)

where K_c is the same as (19):

$K_c = 4$ for simply supported edges,

$K_c = 6.97$ for fully clamped edges.

For combined loading, the buckling condition can be estimated using (Allen and Bulson, 1980; Galambos, 1976):

$$\left(\frac{\sigma}{\sigma^{cr}}\right)^2 + \left(\frac{\tau}{\tau^{cr}}\right)^2 = 1.$$

(25)

Upon substitution of (21)–(24) into (25), the critical condition for core buckling becomes

$$
\left(\frac{V^2}{EM}\right)^{n=1}_{\text{core buckling}} = \frac{\frac{\pi^2 \sin^2\theta}{12(1-v^2)}n^2\left(\frac{d_c}{\ell}\right)^2\left[\frac{d}{\ell}+\frac{n}{6\cos\theta}\frac{d_c}{\ell}\right]}{\left(\frac{H}{\ell}-\frac{d}{\ell}\right)\sqrt{\frac{1}{K_b^2}+\frac{1}{K_s^2}\left(\frac{H}{\ell}-\frac{d}{\ell}\right)^2}\left[\frac{1}{n\tan\theta}\frac{d}{\ell}\frac{\ell}{d_c}+\frac{1}{4\sin\theta}\right]^2} \quad \text{for } n=1, \tag{26a}
$$

$$
\left(\frac{V^2}{EM}\right)^{n=2}_{\text{core buckling}} = \frac{\frac{\pi^2 \sin^2\theta}{12(1-v^2)}n^2\left(\frac{d_c}{\ell}\right)^2\left[\frac{d}{\ell}+\frac{n}{6\cos\theta}\frac{d_c}{\ell}\right]}{\left(\frac{H}{\ell}-\frac{d}{\ell}\right)\sqrt{\frac{1}{K_{cb}^2}+\frac{1}{K_s^2}\left(\frac{H}{\ell}-\frac{d}{\ell}\right)^2}\left[\frac{1}{n\tan\theta}\frac{d}{\ell}\frac{\ell}{d_c}+\frac{1}{4\sin\theta}\right]^2} \quad \text{for } n=2, \tag{26b}
$$

$$
\left(\frac{V^2}{EM}\right)^{n\geqslant 4}_{\text{core buckling}} = \min\left\{\left(\frac{V^2}{EM}\right)^{n\geqslant 4,\text{inner}}_{\text{core buckling}}, \left(\frac{V^2}{EM}\right)^{n\geqslant 4,\text{outer}}_{\text{core buckling}}\right\} \quad \text{for } n\geqslant 4, \tag{26c}
$$

where

$$
\left(\frac{V^2}{EM}\right)^{n\geqslant 4,\text{inner}}_{\text{core buckling}} = \frac{\frac{\pi^2 \sin^2\theta}{12(1-v^2)}n^2\left(\frac{d_c}{\ell}\right)^2\left[\frac{d}{\ell}+\frac{n}{6\cos\theta}\frac{d_c}{\ell}\right]}{\left(\frac{H}{\ell}-\frac{d}{\ell}\right)\sqrt{\frac{1}{K_{cb}^2}\frac{4}{n^2}+\frac{1}{K_s^2}\left(\frac{H}{\ell}-\frac{d}{\ell}\right)^2}\left[\frac{1}{n\tan\theta}\frac{d}{\ell}\frac{\ell}{d_c}+\frac{1}{4\sin\theta}\right]^2}, \tag{27a}
$$

$$
\left(\frac{V^2}{EM}\right)^{n\geqslant 4,\text{outer}}_{\text{core buckling}} = \frac{\frac{\pi^2 \sin^2\theta}{12(1-v^2)}n^2\left(\frac{d_c}{\ell}\right)^2\left[\frac{d}{\ell}+\frac{n}{6\cos\theta}\frac{d_c}{\ell}\right]}{\left(\frac{H}{\ell}-\frac{d}{\ell}\right)\sqrt{\frac{1}{K_c^2}+\frac{1}{K_s^2}\left(\frac{H}{\ell}-\frac{d}{\ell}\right)^2}\left[\frac{1}{n\tan\theta}\frac{d}{\ell}\frac{\ell}{d_c}\right]^2}. \tag{27b}
$$

As for the transverse loading, the influence of the load is fully-embodied within the non-dimensional quantity V^2/EM, but now there are two materials parameters: the yield strain, σ_Y/E, and the Poisson ratio, v.

4. Optimization

The goal is to find the geometric parameters d/ℓ, d_c/ℓ, H/ℓ, n that minimize the weight per unit width subject to a combination of moment and shear force as a function of the load index. The weight of the panel per unit width is given by $W = 2\rho d\ell + n\rho d_c\ell/\cos\theta$, where ρ denotes the density of the material. This weight can be re-written in non-dimensional form as

$$
\psi = \frac{W}{\rho\ell^2} = 2\frac{d}{\ell} + \frac{n}{\cos\theta}\frac{d_c}{\ell}. \tag{28}
$$

To withstand the external load without failing, the stresses in the faces and in the core must be less than the critical values *for all prospective failure modes*. Note that the relative density of the core is

$$
\bar{\rho} = \frac{n}{\cos\theta}\frac{d_c}{H-d}. \tag{29}
$$

The numerical package IMSL has been used to minimize (28), subject to the four constraints.

4.1. Transverse loads

The constraints are

$$
\frac{V^2}{EM}\frac{E}{\sigma_Y}\frac{\ell}{d}\left(\frac{H}{\ell}-\frac{d}{\ell}\right)^{-1}\leqslant 1 \quad \text{face yielding,}
$$

$$
\frac{1}{n\sin\theta}\frac{V^2}{EM}\frac{E}{\sigma_Y}\frac{\ell}{d_c}\leqslant 1 \quad \text{core yielding,}
$$

$$
\frac{48}{k_f\pi^2 n^2 \tan^2\theta}\frac{V^2}{EM}\left(\frac{H}{\ell}-\frac{d}{\ell}\right)\left(\frac{\ell}{d}\right)^3\leqslant 1 \quad \text{face buckling,}
$$

$$
\frac{12}{k_c\pi^2 n^3 \sin^3\theta}\frac{V^2}{EM}\left(\frac{H}{\ell}-\frac{d}{\ell}\right)^2\left(\frac{\ell}{d_c}\right)^3\leqslant 1 \quad \text{core buckling,}
$$

$$(30)$$

where k_f and k_c are given by Eq. (5).

The optimization is performed imposing an upper limit on the core thickness, $H/\ell = 0.2$. Results have been produced for high strength aluminum panels ($\sigma_Y/E = 0.007$) with various values of the order of corrugation ($n = 1, 2, 4, 8$). They reveal that, as the order of corrugation increases from $n = 1$ to $n = 4$, there is a substantial weight reduction (Fig. 6), but minimal additional benefit when n is increased from 4 to 8. As n increases, the optimum face and core thickness decrease, more than compensating for the increase in weight due to the introduction of more core members. Simultaneously, the overall height of the panel increases. Panels made with such material maintain a tolerable panel height ($H/\ell < 0.2$) at the optimal construction. Consequently, the diamond prismatic core (with $n = 4$) has substantially greater structural efficiency than a corrugated core (Fig. 6). Exactly the same analysis has been performed on panels made from a material with small σ_Y/E, such as 304 stainless steel ($\sigma_Y/E = 0.001$): the results showed that optimized diamond core panels exceed reasonable thickness limits and offer no weight benefit.

4.2. Longitudinal loads

The constraints are

$$
\frac{V^2}{EM}\frac{\frac{E}{\sigma_Y}\sqrt{n^2+\frac{3}{\tan^2\theta}\left(\frac{H}{\ell}-\frac{d}{\ell}\right)^2}}{\left[n\frac{d}{\ell}+\frac{n^2}{6\cos\theta}\frac{d_c}{\ell}\right]\left(\frac{H}{\ell}-\frac{d}{\ell}\right)}\leqslant 1,
$$

$$(31a)$$

$$
\frac{V^2}{EM}\left\{\min_{y\in\left[0,\frac{H}{2}-d\right]}\left\{\frac{\frac{\sigma_Y}{E}\left(\frac{H}{\ell}-\frac{d}{\ell}\right)\left[\frac{d}{\ell}+\frac{n}{6\cos\theta}\frac{d_c}{\ell}\right]}{\sqrt{4\left(\frac{y}{H-d}\right)^2+3\left[\frac{1}{n\tan\theta}\left(\frac{H}{\ell}-\frac{d}{\ell}\right)\frac{d}{\ell}\frac{\ell}{d_c}+\frac{1}{\sin\theta}\left(\frac{H}{\ell}-\frac{d}{\ell}\right)\left(\frac{1}{4}-\left(\frac{y}{H-d}\right)^2\right)\right]^2}}\right\}\right\}^{-1}\leqslant 1,
$$

$$(31b)$$

$$
\frac{V^2}{EM}\frac{24(1-\nu^2)}{K_c\pi^2 n^2 \tan^2\theta}\left(\frac{\ell}{d}\right)^2\left(\frac{H}{\ell}-\frac{d}{\ell}\right)\left[\frac{1}{2}\frac{d}{\ell}+\frac{n}{12\cos\theta}\frac{d_c}{\ell}\right]^{-1}\leqslant 1,
$$

$$(31c)$$

$$
\frac{V^2}{EM}\left(\frac{V^2}{EM}\right)^{-1}_{\text{core buckling}}\leqslant 1,
$$

$$(31d)$$

where $(V^2/EM)_{\text{core buckling}}$ is given by Eqs. (26) and (27).

Again, the optimization is performed by imposing an upper limit on the core thickness, $H/\ell = 0.2$. A conservative choice of the buckling coefficients has been made by assuming that the core and face-plates are
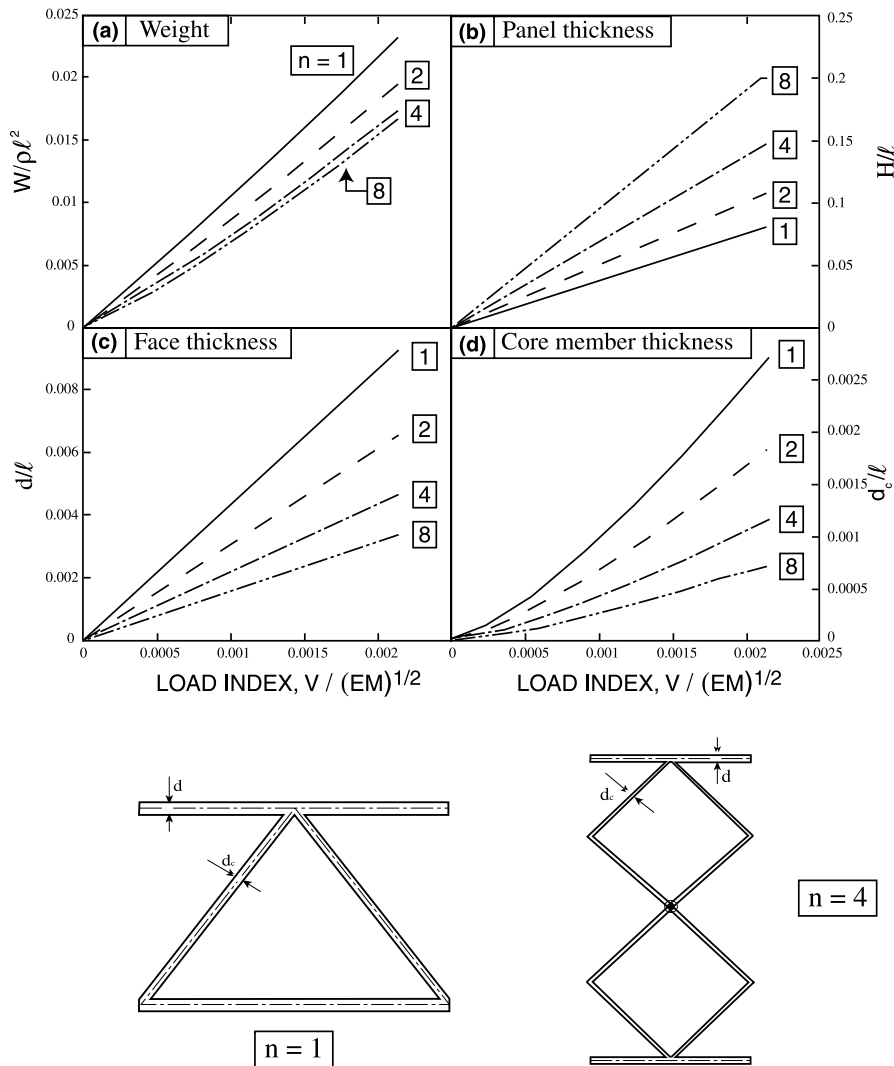
Fig. 6. Effect of the order of corrugation ($n = 1, 2, 4, 8$) on the optimization of prismatic panels loaded in the transverse direction. Results are presented for aluminum alloy panels ($\sigma_Y/E = 0.007$). (a) Minimum weight in non-dimensional form. (b) Optimum panel height normalized by the fundamental length scale $\ell = M/V$. (c) Optimum face thickness, normalized by the characteristic length ℓ. (d) Optimum core member thickness, normalized by the characteristic length ℓ.

simply supported along their long edges (see Section 3.3). For *corrugated core* panels made of high strength Al alloys (Fig. 7), the thickness remains below its allowable level: whereupon the weight remains proportional to the load index. However, for stainless steel, as the load parameter increases, core yielding becomes more prevalent, at the expense of face yielding, causing the maximum allowable core thickness to be reached. This requires that the face thickness be increased to avert failure, causing a rapid increase in the weight. For *diamond panels, there is no benefit in increasing the order of corrugation*. A diamond core panel with $n = 2$ has essentially the same performance as a corrugated core panel at the same weight. Increasing n further decreases the performance at fixed weight (Fig. 7).
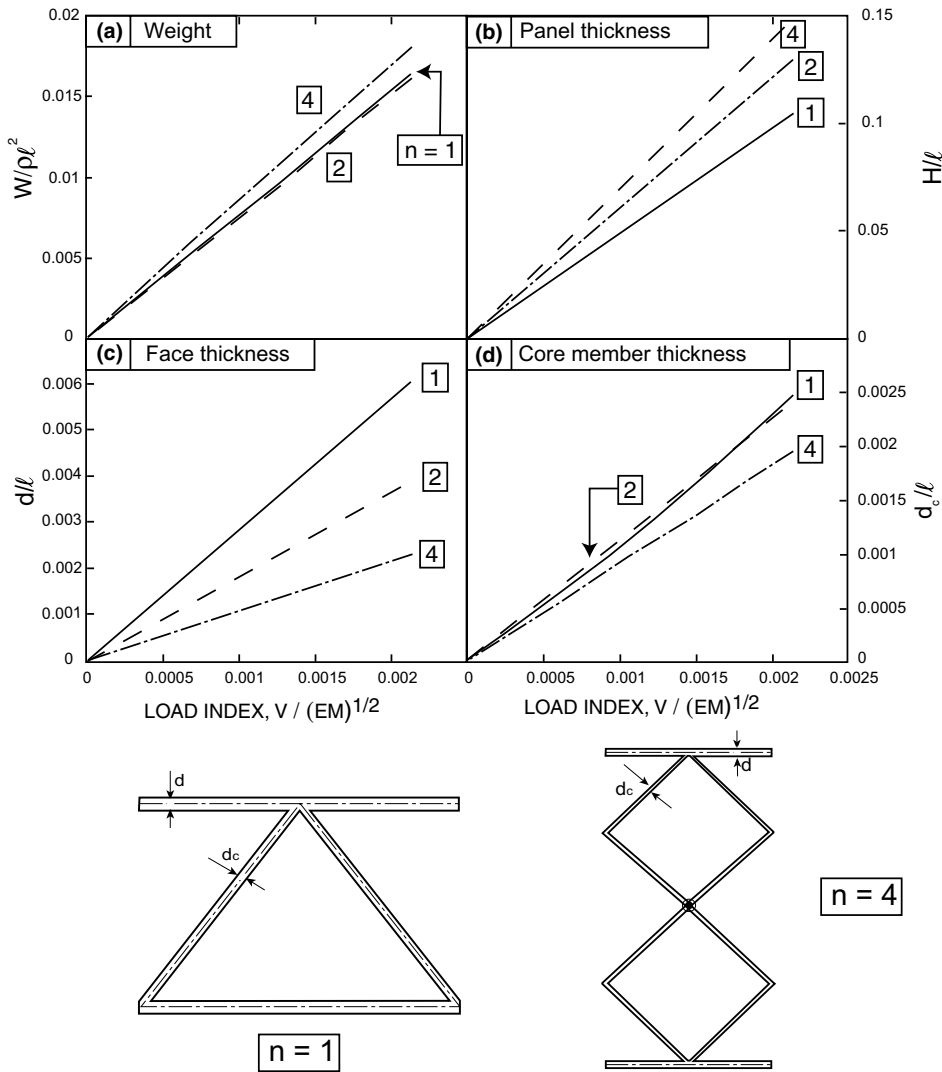
Fig. 7. Effect of the order of corrugation ($n = 1, 2, 4$) on the optimization of prismatic panels loaded in the longitudinal direction. Results are presented assuming Al alloy panels ($\sigma_Y/E = 0.007$). All plates were idealized as simply supported for conservatism. (a) Minimum weight in non-dimensional form. (b) Optimum panel height normalized by the fundamental length scale $\ell = M/V$. (c) Optimum face thickness, normalized by the characteristic length ℓ. (d) Optimum core member thickness, normalized by the characteristic length ℓ.

An interesting consequence of the opposing trends in transverse and longitudinal performance upon increasing the order of corrugation is that panels with $n = 4$, optimally designed for one loading direction, are almost equally weight efficient. Note, however, that the optimized dimensions can differ significantly (see Figs. 6 and 7), implying that a specific panel designed for minimum weight in one loading direction will not perform as well when loaded in the orthogonal direction. Nevertheless, prismatic diamond cores become a realistic option for mutual load bearing and cooling. One extension to be explored in the future would be the optimization of prismatic plates with an isotropy constraint on their strength.

In this analysis, the weight has been minimized under a series of strength constraints, with no attention to stiffness. The same optimization scheme can accommodate stiffness constraints, with the addition of more inequalities to Eqs. (30) and (31). Some of the stiffness related issues are as follows. The vastly different in-plane stiffness of the core in the two loading directions can result in substantial elastic anisotropy. In the transverse direction, the core contributes minimally to the bending stiffness (essentially all the stiffness is provided by the face sheets); whereas in the longitudinal direction the core contribution can be appreciable (depending on the corrugation angle, the order of corrugation and the core member thickness to face sheet thickness ratio). For corrugated core panels ($n = 1$), the difference between the bending stiffness in the longitudinal and transverse loading directions is usually <15%. But, the difference increases as the order of corrugation increases (upon increasing the mass in the core). For $n = 4$ the stiffness in the two directions can differ by a factor of two.

5. Failure maps

Expressing the failure results in terms of maps facilitates visualization. By fixing the non-dimensional weight, ψ, and using H_c/ℓ, d/ℓ as coordinates (H_c represents the height of the core, i.e. $H_c = H - 2d$), the maps identify the load capacities in non-optimal designs, which are often used for various practical considerations (such as minimum-gage limitations (Zok et al., 2003)), as well as providing insight about the responses expected beyond initial failure. For these purposes, superimposed on the maps are contour plots of the non-dimensional load parameter, V^2/EM. Typical maps with $\psi = 0.01$ are presented for a high strength Al alloy: one for transverse loading (Fig. 8a) and the other for longitudinal loading (Fig. 8b). Again, for longitudinal loading, a conservative choice of buckling coefficient has been made (see Section 3.3). The optimal geometry lies at the confluence of face yielding, face buckling, and core buckling. Core yielding is never active for optimized geometries made from this alloy. The core member and face thickness at the optimum can be immediately ascertained from the figures.

6. Finite element comparisons

The accuracy of the analytic results is assessed using the finite element method, using the commercial software ABAQUS. In the *transverse loading* direction, two panels have been studied, a corrugated core panel ($n = 1$) and a diamond core panel ($n = 4$). Both panels were 1 m long, 0.1 m wide, and had a non-dimensional weight $\psi = 0.01$. Both panels were as close as optimum as possible, so that their dimensions can be read from Fig. 6. The panels were modeled using quadratic beam elements. The material is elastic–perfectly plastic and representative of a high strength Al alloy (Young's modulus $E = 70$ GPa, yield strength $\sigma_Y = 490$ MPa ($\sigma_Y/E = 0.007$)). One end of the panel was fully clamped, and the other loaded vertically, in a cantilever mode. No attempt was made to conduct a careful post-buckling study, and the analysis was interrupted shortly after the occurrence of the maximum load. An eigenvalue analysis of the same two panels was also performed, in order to accurately capture the onset of elastic instability (Fig. 9). Notice that including all the members (both those in tension and those in compression) in the computation of the torsional spring stiffness leads to a non-conservative prediction, validating the derivations of Eqs. (3)–(5). The results of the load/displacement calculations are shown in Fig. 10.

For the *longitudinal loading* direction, three panels have been analyzed, one corrugated core panel and two diamond core panels ($n = 2$ and $n = 4$). All the panels were 1 m long, had a non-dimensional weight $\psi = 0.01$ and were nearly optimal. Full 3D unit cell calculations have been performed using with the Riks algorithm and eigenvalue analysis. One end of the panel was clamped (all translation and rotational degrees of freedom were constrained to zero) and the other end displaced vertically, in a cantilever mode. All nodes
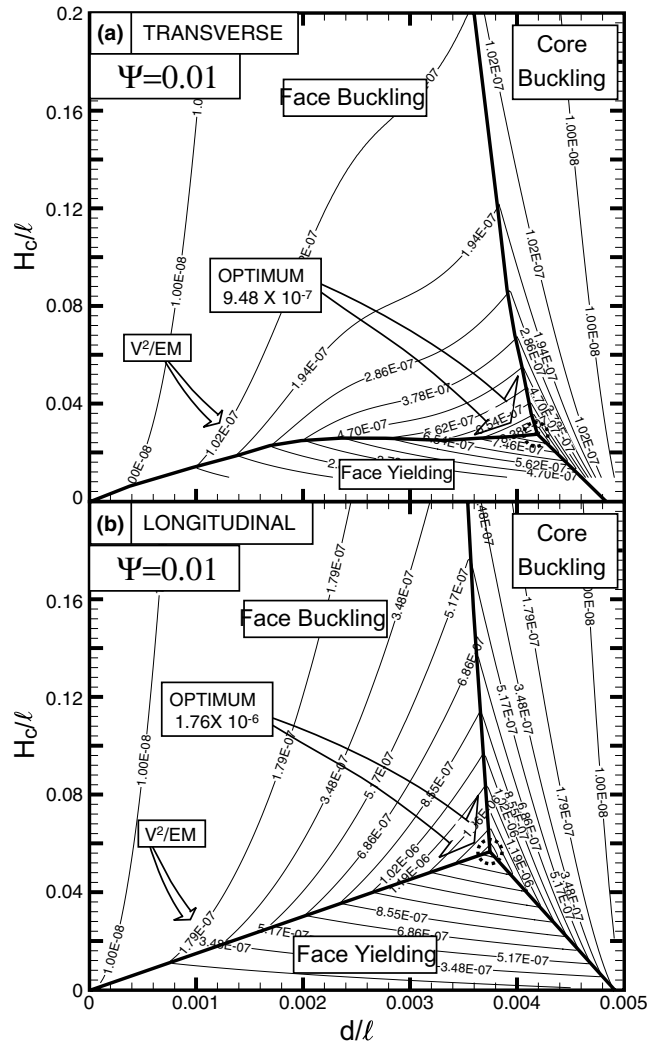
Fig. 8. Prototypical failure maps for corrugated core panels ($n = 1$) made from a high strength Al alloy ($\sigma_Y/E = 0.007$) with $\psi = 0.01$. (a) Loaded in the transverse direction, (b) loaded in the longitudinal direction. Core yielding is never active at reasonable values of d/ℓ and d_c/ℓ when $\psi = 0.01$.

in the loaded section were constrained to displace the same amount in the transverse direction, but allowed to move independently in the longitudinal direction, thus allowing for rotation of the cross section. Quadratic 5-node thin shell elements were employed for both the core and the faces. The results (Figs. 9 and 10) were obtained on unit cell plates (see inset in Fig. 9) with unconstrained long edges; but similar analyses were conducted on larger plates (with more cells across the width) to ensure minimal effects of the boundary conditions on the sides. The eigenvalue analysis confirmed that, when deriving the critical buckling loads, the simply supported plate assumption (see Section 3.3 for details) is indeed conservative (Fig. 9). The load/displacement calculations (Fig. 10) indicate that the load capacities correspond closely with those ascertained analytically.
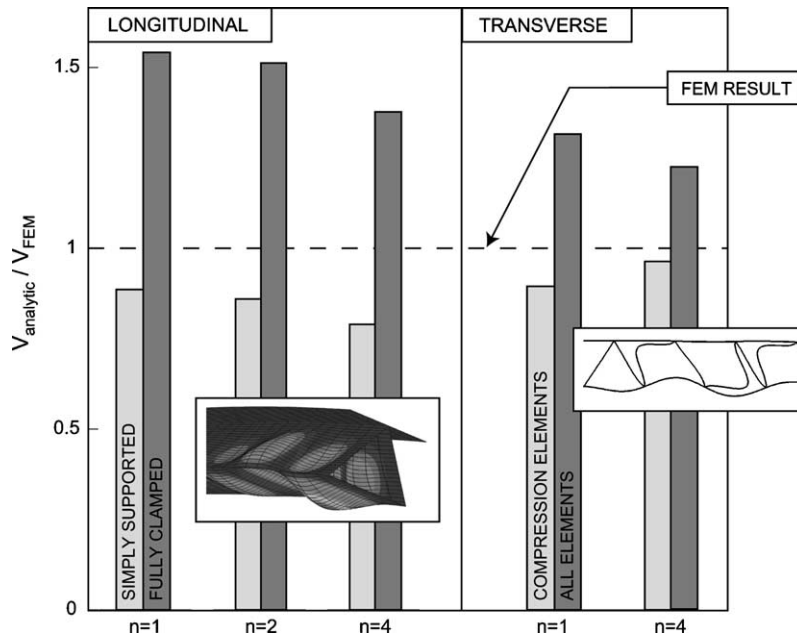
Fig. 9. Comparison of the FEM eigenvalue analysis and the analytic predictions for the buckling critical loads. Note that the inclusion of all members (those in tension and in compression) when computing the torsional stiffness is non-conservative. The insets show typical buckling shapes in both loading directions.
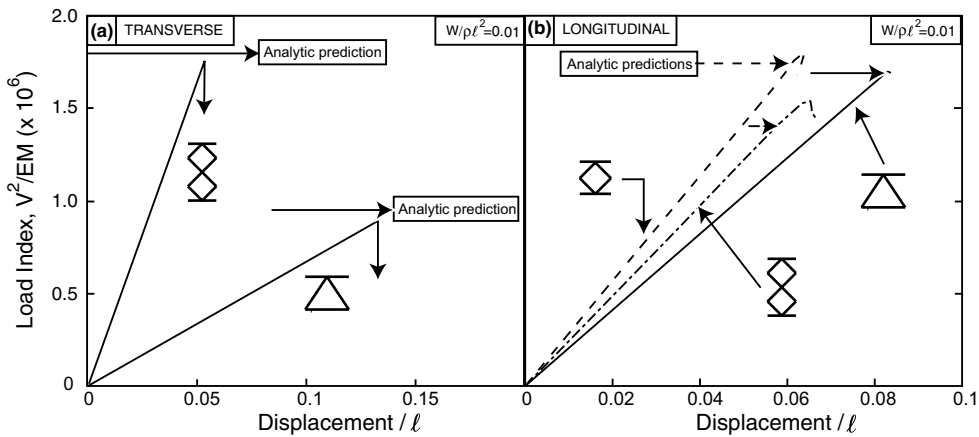

Fig. 10. Numerical load/displacement curves with the load capacities predicted analytically superposed. (a) Two panels loaded in the transverse direction. (b) Three panels loaded in the longitudinal direction.

The load/displacement responses calculated for panels well within one of the buckling regions (far from yielding) indicate the buckling reserve typical of plates (Fig. 11) (Von Karman et al., 1932; Allen and Bulson, 1980; Bazant and Cedolin, 1991). That is, there is no load drop at the onset of elastic buckling. Catastrophic failure only occurs when the buckled area becomes plastic. Designing panels without taking
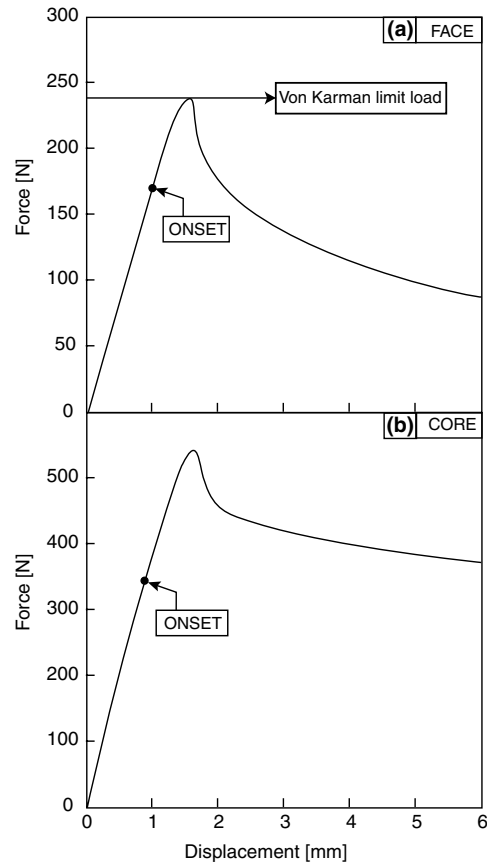
Fig. 11. Finite element calculation showing the post-buckling reserve for a prismatic panel loaded in the longitudinal direction and expected to fail by elastic buckling: (a) face buckling; (b) core buckling.

this phenomenon into account leads to extreme conservatism. An analytic expression for the ultimate load that applies to plates simply supported along the unloaded edges is (Von Karman et al., 1932):

$$\sigma_{ult} = \sqrt{\sigma_Y \cdot \sigma_{cr}}, \tag{32}$$

where σ_{ult} is the average stress induced in the plate by the ultimate load and σ_{cr} is the elastic buckling stress. This formula, due to Von Karman, appears to be in good agreement with the FEM results (Fig. 11a).

Note that the post-buckling reserve would not prove beneficial when optimized panels fail by simultaneous face buckling and face yielding. However, for panels built with high yield strain which are not susceptible to failure by core yielding, the core buckling reserve could shift the boundaries of the failure maps, resulting in lower weight.

7. Implications and conclusions

The optimal dimensions and the minimum weight of sandwich panels with prismatic cores have been evaluated. The corrugated core panel performs best when loaded longitudinally: because, in this orientation, the performance is limited by plate buckling, rather than beam buckling. Superposition of the
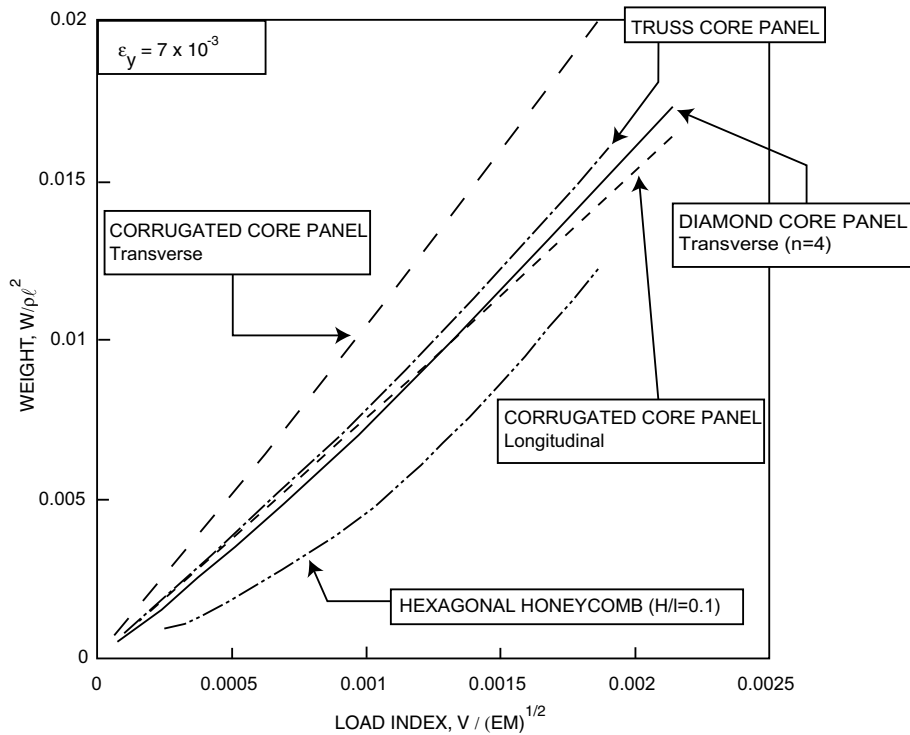
Fig. 12. Comparison of weight efficiency for five different panels: corrugated panels loaded longitudinally, corrugated and diamond panels ($n = 4$) loaded transversely, truss core panels (from Wicks and Hutchinson, 2004) and honeycomb panels (from Wicks and Hutchinson, 2001). All results assume a high strength Al alloy ($\sigma_Y/E = 0.007$).

structural efficiency in the two loading orientations onto results for honeycomb and truss core panels (Fig. 12) demonstrates several features.

 (i) The corrugated core panel has its best performance in the longitudinal orientation, attributable to the greater buckling resistance. For diamond core panels with $n = 4$, the weight efficiency potential is essentially the same in the two loading directions, albeit that the optimized dimensions differ.
 (ii) Honeycomb core panels are more weight efficient than the best prismatic core panels at low load capacity. The benefit diminishes as the load requirement increases.
(iii) The larger the yield strain of the material used to manufacture the panel, the greater the performance, and the larger the benefits of the prismatic core.

The structural attributes of the diamond prismatic core can be combined with its thermal characteristics (Fig. 2) to devise actively cooled multifunctional panels capable of supporting loads while subject to high heat flux. It appears to be among the most weight efficient among open core topologies amenable to active cooling.

References

Allen, H.G., 1969. Analysis and Design of Structural Sandwich Panels. Pergamon Press.
Allen, H.G., Bulson, P.S., 1980. Background to Buckling. McGraw-Hill, London.

Ashby, M.F., Evans, A.G., Fleck, N.A., Gibson, L.J., Hutchinson, J.W., Wadley, H.N.G., 2000. Metal Foams: A Design Guide. Butterworth-Heinemann.

Bazant, Z.P., Cedolin, L., 1991. Stability of Structures. Oxford University Press.

Chiras, S., Mumm, D.R., Evans, A.G., Wicks, N., Hutchinson, J.W., Dharmasena, K., Wadley, H.N.G., Fichter, S., 2002. The structural performance of near-optimized truss core panels. Int. J. Solids Struct. 39 (15), 4093–4115.

Den Hartog, J.P., 1949. Strength of Materials. McGraw-Hill.

Galambos, T.V., 1976. Guide to Stability Design Criteria for Metal Structures, fourth ed. Wiley & Sons.

Gibson, L.J., Ashby, M.F., 1999. Cellular Solids. Structure and Properties. Cambridge University Press.

Gu, S., Lu, T.T., Evans, A.G., 2001. On the design of two-dimensional cellular metals for combined heat dissipation and structural load capacity. Int. J. Heat Mass Transfer 44, 2163–2175.

Leissa, A.W., Kang, J.-H., 2002. Exact solutions for vibration and buckling of an SS-C-SS-C rectangular plate loaded by linearly varying in-plane stresses. Int. J. Mech. Sci. 44, 1925–1945.

Lu, T.J., 2001. Optimal design of a flexural actuator. J. Mech. Phys. Solids 49, 2071–2093.

Southwell, R.V., Skan, S.W., 1924. On the stability under shearing forces of a flat elastic strip. Proc. Royal Soc. London 105 (773), 582–607.

Tall, L., 1974. Structural Steel Design, second ed. The Ronald Press Co., New York.

Von Karman, T., Sechler, E.E., Donnel, L.H., 1932. Strength of thin plates in compression. Trans. Am. Soc. Mech. Eng. 54, 53.

Wicks, N., Hutchinson, J.W., 2001. Optimal truss plates. Int. J. Solids Struct. 38, 5165–5183.

Wicks, N., Hutchinson, J.W., 2004. Performance of sandwich plates with truss cores. Mechanics of Materials 36 (8), 739–751.

Wiernicki, C.J., Liem, P.E., Woods, G.D., Furio, A.J., 1991. Structural analysis methods for lightweight metallic corrugated core sandwich panels subjected to blast loads. Naval Eng. J. 103, 192–203.

Zok, F.W., Rathbun, H.J., Wei, Z., Evans, A.G., 2003. Design of metallic textile core sandwich panels. Int. J. Solids Struct. 40, 5707–5722.